Image Registration Using
Multi-Scale Texture Moments

Jun Sato and Roberto Cipolla

CUED/F-INFENG/TR 177

October 1994

This paper will appear in the special issue of
Image and Vision Computing journal in 1995.

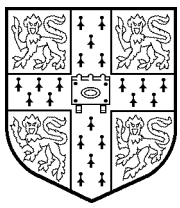

Department of Engineering
University of Cambridge
Trumpington Street
Cambridge CB2 1PZ
England

Email: js2@eng.cam.ac.uk

Image Registration Using Multi-Scale Texture Moments

Jun Sato and Roberto Cipolla
Department of Engineering,
University of Cambridge
Cambridge CB2 1PZ, England.

October 1994

Abstract

In this paper we propose a novel, efficient and geometrically intuitive method to compute the four components of an affine transformation from the change in simple statistics of images of texture. In particular, we show how the changes in second circular moments of edge orientation are directly related to the rotation (curl), scale (divergence) and deformation components of an affine transformation, and how these components can be computed from multi-scale texture moments. A simple implementation is described which does not require point, edge or contour correspondences to be established. It is tested on repetitive and non-repetitive visual textures which are neither isotropic nor homogeneous. The theoretical accuracy and the noise sensitivity of this method are compared with other linear moment and circular moment methods.

Keywords: texture moments, affine transformation, multi-scale, image registration, visual motion

1 Introduction

Structure from motion (or stereo) and shape from texture can sometimes be conveniently analysed in a two stage framework. The first stage involves the estimation of image velocities (disparities) in structure from motion (stereo) or *texture gradients* in shape from texture [1]. The second stage involves their interpretation to infer the viewer motion and/or the distance and shape of the visible surfaces.

In structure from motion, relative motion between the viewer and scene induces distortion in image detail and apparent shape. In small neighbourhoods and for smooth surfaces this distortion – the image velocity field or disparity field – can be conveniently described by an image translation and a four parameter *affine (linear) transformation* [2, 3]. In shape from texture, the distortion in a given direction of an image of a surface with a repeated texture pattern – texture gradients – can also be modelled by affine transformations [4, 5].

The estimation of an affine transformation is often an integral part in recovering the image velocity field and *distortion map*. Better still, the affine transformation can be decomposed into an image translation, a change in scale (divergence), an image rotation (curl) and a shear (deformation) [2] which are related to the scene structure and viewer's motion in a simple, geometrically intuitive way.

Many methods have been proposed in the literature to extract the affine transformations from an image sequence (structure from motion) or between different parts of a single image (shape from texture). These can be broadly divided into methods which require the correspondence of features or tokens, and methods which exploit the temporal coherence in an image sequence and avoid the correspondence problem.

The simplest method is based on the accurate extraction of points or corner features and their correspondences [6]. The image motion of a minimum of three points (provided they are not colinear) is sufficient to completely define the affine transformation. Unfortunately, many corner finders produce poorly localised features which are often temporally unstable [7, 8, 9, 10, 11], although clusters of corners can be used [12]. The technology for edge detection is more advanced than isolated point detection. Reliable, accurate edge detectors, which localise surface markings to sub-pixel accuracy [13], can be used to recover the normal (vernier) component of velocity at edges. A minimum of six normal velocities can then be used to compute the affine transformation [14, 15]. Both corner and edge tracking require finding correspondences over the image sequence. This becomes a non-trivial problem when the image motion is large or in densely textured images. Cipolla and Blake [16] presented a novel method to recover the affine transformation of a deforming closed contour from the integral of simple functions of the normal image velocities around the contour. This integration provided some immunity to image measurement noise. This is equivalent to measuring the temporal changes in the area of a closed contour. Although this method did not require point or line correspondences, the extraction and tracking of closed contours is also not always possible in richly textured images.

A large number of techniques have been developed which avoid the extraction and explicit correspondence of tokens or features. For small visual motions or distortions, a common method is to estimate the affine transform from spatiotemporal gradients of image intensity from the motion constraint equation [17, 18, 19]. The amount of visual motion allowed (especially rotation) is limited by the smoothing scale factor. For larger image motions, brute force search techniques have been used [20].

For estimating the texture distortion map, Malik and Rosenholtz [5] and others [21, 22] have attempted to solve for the affine transformation in the Fourier domain, although this involves the choice of a suitable window and is computationally expensive. A more common approach exploits the *second moment* statistics of image edge orientations. Under the assumptions of directional isotropy [23] in the real texture, it is possible to estimate the surface orientation from the second moment matrix of image element orientations [24, 25, 26]. Modifications of the second moment matrix, which also exploit image intensity gradients, have also been used [27, 28]. It is, of course, impossible to recover the affine transformation (four independent parameters) uniquely from the second moment matrix (which is symmetric and positive semidefinite). (This is equivalent to the "aperture problem in the large" [29] when trying to distinguish the rotation (curl) and pure shear components (deformation) in the distortion of an ellipse under small viewer motions.) In many existing schemes, restrictions on the class of texture – isotropy or homogeneity – or on the stereo geometry [28] allow an incomplete solution. In Malik and Rosenholtz's work [5] all four affine parameters are needed to completely specify surface position and 3D shape for a general repetitive texture. All four parameters of the affine transformation are also required for an arbitrary stereo configuration or in structure from motion.

Recently, a novel method [30] was proposed to compute all four parameters of the affine transformation from simple linear moments. Although this method succeeds in deriving the affine transformation of texture images which are neither isotropic nor homogeneous, it suffers from the aliasing problem, that is the distribution of orientation is not continuous at 0 and π radians, and the theory breaks down at these points. Although this problem can be avoided by using circular moments, second circular moments are not sufficient to compute all the four parameters of affine transformation. One solution is to use higher moments, but these are sensitive to noise.

In this paper, we propose a novel, efficient and geometrically intuitive method to compute the four components of an affine transformation only from the change in second circular moments of the images of texture using multi-scale-space representations. This method does not require any correspondence of the image feature to be established, and does not suffer from the aliasing problem. The theoretical accuracy and noise sensitivity of this method are compared with other linear and circular moment methods. A simple implementation is

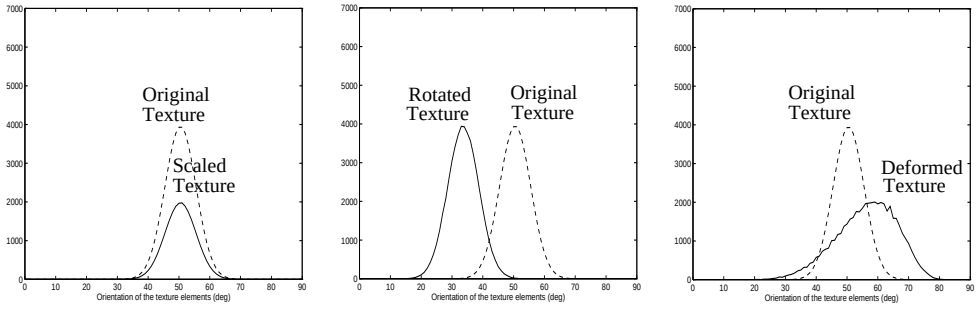

(a) (b) (c)

Figure 1: Distribution of the orientation of the original and distorted texture elements. The original distribution is shown by a dashed line in each graph and the distribution changed by scaling, rotation and deformation are shown by solid lines in (a), (b) and (c) respectively. The original distribution is a Gaussian distribution of 50000 elements with mean value of 50 degrees and standard deviation of 9 degrees. The scale factor used in (a) is 0.7, the rotation used in (b) is -15 degrees, and the magnitude and axis of deformation used in (c) are 1.5 and 80 degrees respectively. Scaling does not change the shape of the orientation distribution but changes its area (a). Rotation changes the mean value of the distribution (b). Deformation changes the variance and skewness of the distribution (c).

described, and is tested on repetitive and non-repetitive visual textures which are neither isotropic nor homogeneous.

2 Approach

In this section, we show how the moments of orientation of the texture elements are closely related to the components of an affine transformation, and how the moments of multi-scale images can be used to recover the affine transformation.

Consider the texture to have oriented elements with distribution, $f(\varphi)$, which will be changed to $f'(\varphi)$ by an affine transformation. An affine transformation can be described by the four components, that is an isotropic scale, rotation, magnitude of deformation and axis of deformation. As shown in Fig.1 (a), if the scale is changed, the distribution, $f(\varphi)$, changes similarly, that is the zeroth moment of $f(\varphi)$ is changed but any higher moments are not affected. The rotation, as shown in Fig.1 (b), changes the orientations of the texture elements equally. This means that rotation is related to a shift in the mean value of $f(\varphi)$ (i.e. the first moment of $f(\varphi)$), and does not affect the zeroth moment or higher moments. The deformation term, on the other hand, depends on the original orientation of the element and hence affects the variance of $f(\varphi)$ (i.e. the second moment of $f(\varphi)$) as shown in Fig.1 (c). Furthermore, the changes in the distribution of orientation will not generally be symmetric about the mean of the orientations, and hence the skewness of $f(\varphi)$ (i.e. the third moment of $f(\varphi)$) will be affected. Thus, we can compute all affine components, that is change in scale, rotation and deformation, from the zeroth, first, second and third moments of orientation of the texture elements. This linear moments method was proposed in [30].

The linear moments, however, suffer from an aliasing problem, arising from the fact that the distribution of orientation is not continuous at 0 and π radians (see Fig.2). Because we use the changes in distribution for computation of an affine transformation, the translation of the distribution over 0 or π radians can cause a serious error in computation of the affine components.

Fortunately, this problem can be avoided by using circular moments, which are continuous. As described in the previous section, second circular moments are not sufficient to recover all

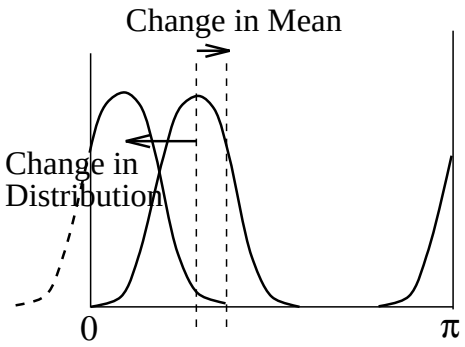

Figure 2: Aliasing problem of linear moments of orientation. If the distribution translate over 0 or π radians by an affine transformation, the change in moments (e.g. change in mean value) are no longer consistent with the change in distribution itself.

four components of an affine transformation, because the second circular moments include just two individual segments. Although we can solve the problem using higher circular moments, these are sensitive to noise and are not always reliable.

On the other hand, research in scale-space theory [31, 32, 33, 34] shows we can exploit different image features in an image by choosing different scales. Further more, recent work has developed diffusion processes for multi-scale representation which preserve an affine transformation, that is an *affine invariant scale-space* [35, 36]. If the diffusion process is affine invariant, image features extracted at different scales in an image distorted by an affine transformation belong to physically different image structures, but are distorted by the same affine transformation. This means we can obtain different information about the same affine transformation by choosing different scales in a diffusion process. This is demonstrated in Fig.3 which shows the original and distorted images at different scales derived by an affine invariant diffusion process [35].

In the next section, we describe how we can compute all four components of the affine transformation reliably, without any correspondence, using two or more scale-space representations.

3 Theoretical Framework

In this section, we formalize the method of computing the parameters of an affine transformation from the moments of multi-scale representation. To do this, we first show that the affine transformation can be computed using differential invariants of the image velocity field. Next, we describe how the change in orientation of the image detail is related to the parameters of an affine transformation. This observation is then used to derive the relationship between these parameters and the moments of the orientation of image detail. Unfortunately, this relationship provides only two equations, but there are four unknown parameters of the affine transformation. To compute the affine parameters uniquely, we combine this relationship with multi-scale-space representation, and formalize the method to compute all four parameters of an affine transformation from the moments of the orientation of image detail in closed form.

3.1 Differential Invariants of the Image Velocity Field

Generally, an affine transformation, A, which represents the image distortion, can be described by the 2×2 identity matrix, I, and a 2×2 differential component, Q, as follows:

$$A = I + Q \tag{1}$$

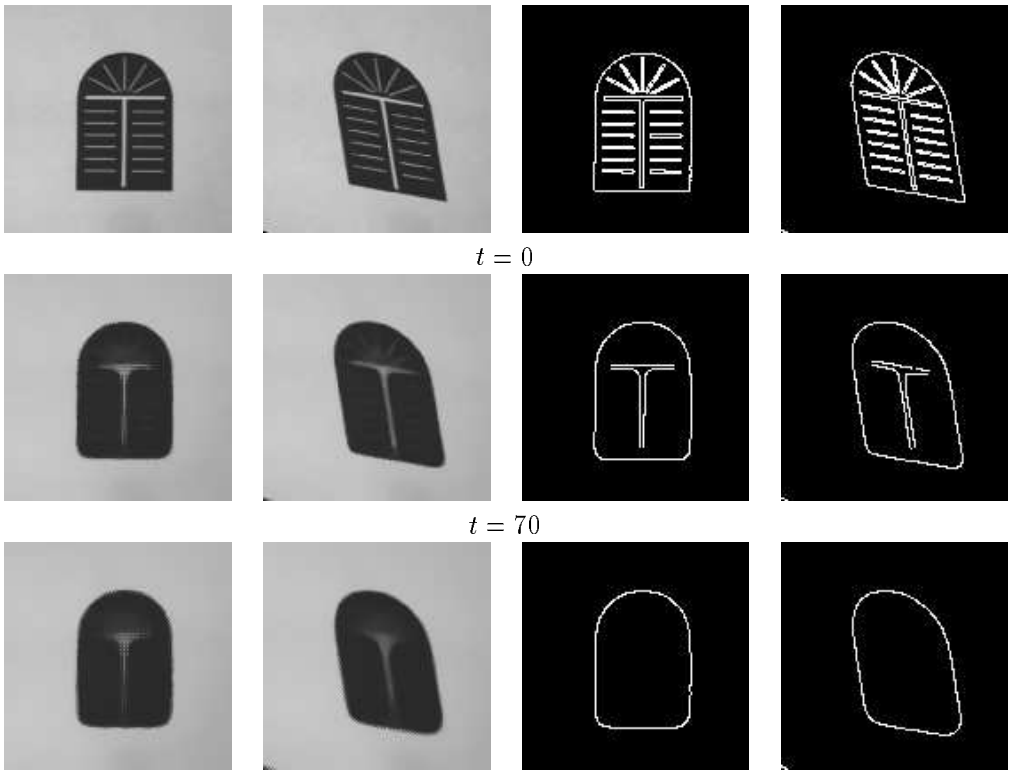

Figure 3: Original and distorted multi-scale images and their edges. The images in column (a) are the original images represented at three different scales. Column (b) shows the same images distorted by an affine transformation. The affine transformation is equivalent to the transformation in viewing a fronto-parallel textured surface which has been rotated to have a slant of 45 degrees and a tilt of -45 degrees. The images in the second and third row of columns (a) and (b) are derived from the images in the top row by an affine invariant diffusion process developed by Lopez and Morel [35] with scales (variances) of $t = 70$ and $t = 240$ respectively. The images in columns (c) and (d) show edges derived from the images in columns (a) and (b) respectively. We find that different information about the same affine transformation can be obtained by choosing different scale-space representations.

If the image distortion is small, the differential component, Q, of the affine transformation can be approximated by the first order partial derivatives of the image velocity field:

$$Q = \begin{bmatrix} u_x & u_y \\ v_x & v_y \end{bmatrix}$$

where u_x, u_y, v_x and v_y are the partial derivatives of the image velocity, $\mathbf{v} = [u(x,y), v(x,y)]$. It is well known that the matrix Q can be decomposed into the first order differential invariants of the image velocity field, i.e. divergence, curl and deformation [16]:

$$Q = \frac{\mathrm{div}\mathbf{v}}{2}\begin{bmatrix} 1 & 0 \\ 0 & 1 \end{bmatrix} + \frac{\mathrm{curl}\mathbf{v}}{2}\begin{bmatrix} 0 & -1 \\ 1 & 0 \end{bmatrix} + \frac{\mathrm{def}\mathbf{v}}{2}\begin{bmatrix} \cos 2\mu & \sin 2\mu \\ \sin 2\mu & -\cos 2\mu \end{bmatrix} \tag{2}$$

where μ is the orientation of the axis of maximum expansion. div$\mathbf{v}$, curl$\mathbf{v}$ and def$\mathbf{v}$ are the divergence, curl and deformation components of the image velocity field, $\mathbf{v}$, and defined by:

$$\begin{aligned} \mathrm{div}\mathbf{v} &= u_x + v_y \\ \mathrm{curl}\mathbf{v} &= -u_y + v_x \\ \mathrm{def}\mathbf{v}\cos 2\mu &= u_x - v_y \\ \mathrm{def}\mathbf{v}\sin 2\mu &= u_y + v_x \end{aligned}$$

The advantage of representing an affine transformation using the first order differential invariants is not only its simplicity, but also its direct relationship to the three dimensional configuration. In structure from motion the relationship between the viewer motion and the surface orientation can be described using these differential invariants as shown in [16]. Therefore, once the differential invariants of the image velocity field have been computed, we can partially solve the motion of the observer and the structure of the scene. These solutions are not complete, but are enough for some applications such as time-to-contact in visual navigation.

3.2 Changes in Image Orientation and the Affine Transformation

In this section, we investigate the effect of the first order differential invariants on the orientation of image detail. In the next section, we use this results to derive the relationship between texture moments and an affine transformation.

Consider an element of texture represented by a unit vector, $\mathbf{v}$, with orientation, φ. As shown in Fig.4, the affine transformation, A, transforms the vector, $\mathbf{v}$, into $\mathbf{v}'$ with orientation φ'. Therefore, the x and y component of the transformed vector, $\mathbf{v}'$, is described as follows:

$$\begin{aligned} \begin{bmatrix} L'(\varphi)\cos\varphi' \\ L'(\varphi)\sin\varphi' \end{bmatrix} &= A\mathbf{v} \\ &= \begin{bmatrix} 1+s+d_1 & d_2-c \\ d_2+c & 1+s-d_1 \end{bmatrix}\begin{bmatrix} \cos\varphi \\ \sin\varphi \end{bmatrix} \end{aligned} \tag{3}$$

where $L'(\varphi)$ is the length of $\mathbf{v}'$ (note that the transformed vector is no longer a unit vector) and is computed by (see Appendix A):

$$L'(\varphi) \simeq 1 + d_1\cos 2\varphi + d_2\sin 2\varphi + s \tag{4}$$

and for simplification we changed the expression of the differential invariants as follows:

$$\begin{aligned} s &= \frac{1}{2}\mathrm{div}\mathbf{v} \\ c &= \frac{1}{2}\mathrm{curl}\mathbf{v} \\ d_1 &= \frac{1}{2}\mathrm{def}\mathbf{v}\cos 2\mu \\ d_2 &= \frac{1}{2}\mathrm{def}\mathbf{v}\sin 2\mu \end{aligned}$$

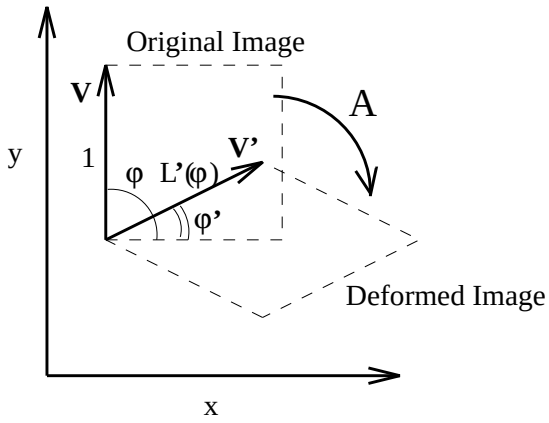

Figure 4: Change in orientation and length of a texture element under an affine transformation. A unit vector, $\mathbf{v}$, with orientation φ, is changed to vector $\mathbf{v}'$, with orientation φ' and length $L'(\varphi)$, by an affine transformation, A.

We now compute $\cos 2\varphi'$ and $\sin 2\varphi'$, because we will use second circular moments in the next stage. (Note that first circular moments are always zero, because we reflect each orientation, φ, of the image detail to $\varphi+\pi$ before computing the moments to avoid an aliasing problem. This is described in the next section and Appendix B.) From (3), $\cos 2\varphi'$ and $\sin 2\varphi'$ are computed by:

$$\begin{aligned}
\cos 2\varphi' &= \cos^2\varphi' - \sin^2\varphi' \\
&= \frac{1}{L'(\varphi)^2}\left(k_{11}\cos 2\varphi + k_{12}\sin 2\varphi + k_{13}\right) \qquad (5)\\
\sin 2\varphi' &= 2\sin\varphi'\cos\varphi' \\
&= \frac{1}{L'(\varphi)^2}\left(k_{21}\sin 2\varphi + k_{22}\cos 2\varphi + k_{23}\right) \qquad (6)
\end{aligned}$$

where:

$$\begin{aligned}
k_{11} &= 1 + d_1^2 - d_2^2 + s^2 + 2s - c^2 \\
k_{12} &= 2(d_1 d_2 - c - cs) \\
k_{13} &= 2(d_1 + d_1 s - d_2 c) \\
k_{21} &= 1 - d_1^2 + d_2^2 + s^2 + 2s - c^2 \\
k_{22} &= 2(d_1 d_2 + c + cs) \\
k_{23} &= 2(d_2 + d_2 s + d_1 c)
\end{aligned}$$

If the image distortion is small, that is $s \ll 1$, $c \ll 1$, $d_1 \ll 1$ and $d_2 \ll 1$, the second order products of these differential invariants can be neglected. Then, (5) and (6) are approximated to first order by:

$$\cos 2\varphi' \simeq \frac{1}{L'(\varphi)^2}\left(\cos 2\varphi + 2s\cos 2\varphi - 2c\sin 2\varphi + 2d_1\right) \qquad (7)$$

$$\sin 2\varphi' \simeq \frac{1}{L'(\varphi)^2}\left(\sin 2\varphi + 2s\sin 2\varphi + 2c\cos 2\varphi + 2d_2\right) \qquad (8)$$

3.3 Texture Moments under Affine Transformation

In this section, we formalize the relationship between the circular moments of the orientation of the texture and the four components of the affine transformation. This allows us to compute

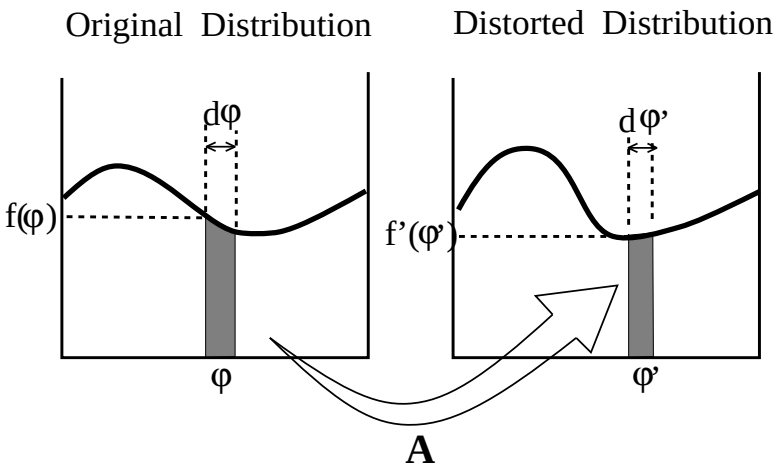

Figure 5: Change in distribution of orientation of texture elements under an affine transformation. The small interval, $(\varphi,\ \varphi + d\varphi)$, of the original distribution, $f(\varphi)$, moves to the small interval, $(\varphi',\ \varphi' + d\varphi')$, of the distorted distribution, $f'(\varphi')$, by an affine transformation, A.

an affine transformation without any correspondence of spatial image features. In previous work on shape from texture, the texture was often assumed either to be spatially homogeneous or isotropic in orientation, though such textures are limited in the real world. Here, we consider any visual pattern in the real world as a texture, and consider the change in the statistics of the visual texture under an affine transformation.

Consider the texture to have oriented elements with distribution, $f(\varphi)$, which will be changed to $f'(\varphi')$ by an affine transformation. As shown in Fig.5, the unit texture elements whose orientations lie in the small interval $(\varphi,\ \varphi + d\varphi)$ move to the small interval $(\varphi',\ \varphi' + d\varphi')$ by the affine transformation, and the length of the each element is changed to $L'(\varphi)$. Then, the number of unit elements, $g(\varphi')$ which lie in the interval $(\varphi',\ \varphi' + d\varphi')$ is described as follows:

$$g(\varphi')d\varphi' \quad = \quad L'(\varphi)f(\varphi)d\varphi$$

Because $f'(\varphi')$ and $f(\varphi)$ are defined per unit area, the transformed distribution $f'(\varphi')$ is described as follows:

$$\begin{aligned} f'(\varphi')d\varphi' &= \frac{T}{T'}g(\varphi')d\varphi' \\ &= \frac{T}{T'}L'(\varphi)f(\varphi)d\varphi \end{aligned} \tag{9}$$

where T and T' are the total length of the texture elements in the original and deformed area. The moment , $I_{F(\varphi')}$, of an arbitrary function, $F(\varphi')$, of the deformed texture with distribution, $f'(\varphi')$, can therefore be described as follows:

$$\begin{aligned} I_{F(\varphi')} &= \int_0^{2\pi} F(\varphi')f'(\varphi')d\varphi' \\ &= \frac{T}{T'}\int_0^{2\pi} F(\varphi')L'(\varphi)f(\varphi)d\varphi \end{aligned} \tag{10}$$

This is a general expression of the moment of the texture deformed by an affine transformation.

By definition, nth order circular moments, $I_{\sin n\varphi}$, $I_{\cos n\varphi}$, of the orientation, φ, of the

texture element are described as follows [37]:

$$I_{\sin n\varphi} = \int_0^{2\pi} \sin n\varphi f(\varphi) d\varphi \tag{11}$$

$$I_{\cos n\varphi} = \int_0^{2\pi} \cos n\varphi f(\varphi) d\varphi \tag{12}$$

where, $f(\varphi)$ is the distribution function of orientation of the texture element. In practice, because φ and $\varphi + \pi$ cannot be distinguished, odd order circular moments (e.g. 1st, 3rd circular moments) are always zero (see Appendix B). Therefore, even order moments (e.g. 2nd, 4th circular moments) are necessary to compute the affine transformation.

Second circular moments of the deformed texture, $I_{\sin 2\varphi'}$ and $I_{\cos 2\varphi'}$ can be described from (11), (12) and (10) as follows:

$$\begin{aligned} I_{\sin 2\varphi'} &= \int_0^{2\pi} \sin 2\varphi' f'(\varphi') d\varphi' \\ &= \frac{T}{T'} \int_0^{2\pi} \sin 2\varphi' L'(\varphi) f(\varphi) d\varphi \end{aligned} \tag{13}$$

$$\begin{aligned} I_{\cos 2\varphi'} &= \int_0^{2\pi} \cos 2\varphi' f'(\varphi') d\varphi' \\ &= \frac{T}{T'} \int_0^{2\pi} \cos 2\varphi' L'(\varphi) f(\varphi) d\varphi \end{aligned} \tag{14}$$

Substituting (7) and (8) into (13) and (14):

$$I_{\sin 2\varphi'} = \frac{T}{T'} \int_0^{2\pi} (\sin 2\varphi + 2s \sin 2\varphi + 2c \cos 2\varphi + 2d_2) \frac{1}{L'(\varphi)} f(\varphi) d\varphi \tag{15}$$

$$I_{\cos 2\varphi'} = \frac{T}{T'} \int_0^{2\pi} (\cos 2\varphi + 2s \cos 2\varphi - 2c \sin 2\varphi + 2d_1) \frac{1}{L'(\varphi)} f(\varphi) d\varphi \tag{16}$$

Because $L'(\varphi) \simeq 1$ under small image distortion, $1/L'(\varphi)$ of (15) and (16) can be approximated to first order by:

$$\frac{1}{L'(\varphi)} \simeq 1 - (L'(\varphi) - 1) \tag{17}$$

Substituting (4) and (17) into (15) and (16), and approximating to first order by neglecting the second order products of the differential invariants, second circular moments of the deformed texture are described by second and fourth circular moments of the original texture as follows:

$$I_{\sin 2\varphi'} \simeq \frac{T}{T'} (I_{\sin 2\varphi} + s I_{\sin 2\varphi} + 2c I_{\cos 2\varphi} - \frac{d_1}{2} I_{\sin 4\varphi} + \frac{d_2}{2} (3 + I_{\cos 4\varphi})) \tag{18}$$

$$I_{\cos 2\varphi'} \simeq \frac{T}{T'} (I_{\cos 2\varphi} + s I_{\cos 2\varphi} - 2c I_{\sin 2\varphi} + \frac{d_1}{2} (3 - I_{\cos 4\varphi}) - \frac{d_2}{2} I_{\sin 4\varphi}) \tag{19}$$

where $I_{\sin 2\varphi}$, $I_{\cos 2\varphi}$, $I_{\sin 4\varphi}$ and $I_{\cos 4\varphi}$ denote second and fourth circular moments of the original texture respectively. Note that the moments of the deformed texture are described by simple linear combination of the moments of the original texture.

3.4 Multi-Scale Texture Moments

In the previous section, we derived the relationship between the moments of the texture and the components of the affine transformation. We have only two equations, and there are four unknown parameters in these equations, i.e. four components of the affine transformation.

Due to this lack of constraints, we cannot compute the affine components uniquely from the moments of the texture. In this section, we propose an efficient method to compute four components of the affine transformation reliably, using the moments of scale-space representations of the image.

As shown in the literature [31, 33], we can observe the different image structures in one image using scale-space representation: a certain scale extracts a certain structure in the image and a different scale extracts a different structure. Image features extracted by different scales in an image distorted by an affine transformation belong to physically different image structures, but are distorted by the same affine transformation. This means we can automatically obtain moments which are derived from different image features but are affected by the same affine transformation by choosing different scale-space representations. Combining two or more scale-space representations with derived equations of moments and the affine transformation, we can compute all four components of the affine transformation directly and reliably without any correspondence.

Consider two different scale-space representations, whose scales are t_1 and t_2, to have different texture moments defined by (13), (14), that is $I_{\sin 2\varphi_1}$ and $I_{\cos 2\varphi_1}$ for t_1 and $I_{\sin 2\varphi_2}$ and $I_{\cos 2\varphi_2}$ for t_2, and these moments are changed to $I_{\sin 2\varphi_1'}$, $I_{\cos 2\varphi_1'}$, $I_{\sin 2\varphi_2'}$ and $I_{\cos 2\varphi_2'}$ by the affine transformation. Then, from (18) and (19), the relationship between these texture moments and the components of the affine transformation can be described as follows:

$$\begin{bmatrix} \frac{T_1'}{T_1} I_{\cos 2\varphi_1'} - I_{\cos 2\varphi_1} \\ \frac{T_1'}{T_1} I_{\sin 2\varphi_1'} - I_{\sin 2\varphi_1} \\ \frac{T_2'}{T_2} I_{\cos 2\varphi_2'} - I_{\cos 2\varphi_2} \\ \frac{T_2'}{T_2} I_{\sin 2\varphi_2'} - I_{\sin 2\varphi_2} \end{bmatrix} = \begin{bmatrix} I_{\cos 2\varphi_1} & -2I_{\sin 2\varphi_1} & \frac{1}{2}(3 - I_{\cos 4\varphi_1}) & -\frac{1}{2} I_{\sin 4\varphi_1} \\ I_{\sin 2\varphi_1} & 2I_{\cos 2\varphi_1} & -\frac{1}{2} I_{\sin 4\varphi_1} & \frac{1}{2}(3 + I_{\cos 4\varphi_1}) \\ I_{\cos 2\varphi_2} & -2I_{\sin 2\varphi_2} & \frac{1}{2}(3 - I_{\cos 4\varphi_2}) & -\frac{1}{2} I_{\sin 4\varphi_2} \\ I_{\sin 2\varphi_2} & 2I_{\cos 2\varphi_2} & -\frac{1}{2} I_{\sin 4\varphi_2} & \frac{1}{2}(3 + I_{\cos 4\varphi_2}) \end{bmatrix} \begin{bmatrix} s \\ c \\ d_1 \\ d_2 \end{bmatrix}$$

where T_1 and T_2 are the total length of the original texture elements in the scale t_1 and t_2, and T_1' and T_2' are those of the deformed texture elements. We can compute four differential components, s, c, d_1, d_2, of the affine transformation as a solution to this matrix equation. The absolute components of the affine transformation are computed using the derived differential components and (1). This method requires minimal information to compute an affine transformation using two different scales. We can also use more than two scales and raise the accuracy and robustness of this method.

The properties of the proposed method are:

1. It does not require correspondence of individual image features.
2. This allows much greater interframe motions than spatio-temporal techniques.
3. The method relies on the comparison of statistics of the image patches. This will only be meaningful if the two patches are projections of "world" textures with similar properties. This therefore requires that corresponding areas of interest are identified.
4. This method does not suffer from an aliasing problem which occurs when linear moments are used.

4 Theoretical Accuracy and Noise Sensitivity

In this section we compare the systematic error and sensitivity to noise of this method with those of the linear moments method [30] and another circular moment method, Kanatani's Buffon transform method [26]. Kanatani's method uses the relationship between the coefficients of the Fourier series of the inverse Buffon transform and the Fourier coefficients of the distribution of orientation of image features, and is used to compute slant, tilt and rotation of a surface.

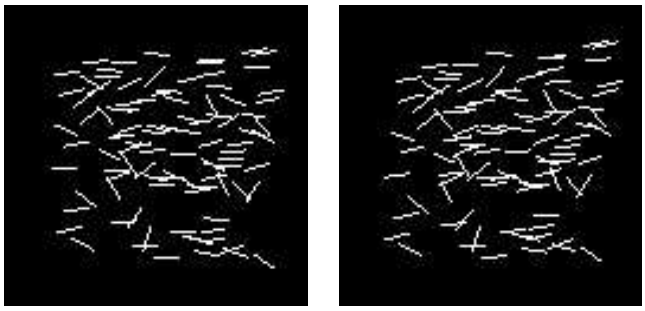

(a) (b)

Figure 6: Texture elements used in the error and noise sensitivity analysis. (a) shows the original data used in the experiments with 100 texture elements whose orientations are from a Gaussian distribution with a mean of 0 degrees and a standard deviation of 30 degrees. (b) shows a typical data set of the distorted texture elements. In this example, texture elements are distorted by an affine transformation with a magnitude of deformation of 30 degrees and an axis of deformation of 45 degrees.

4.1 Comparison of Systematic Error

All three methods use approximations to solve the problem in closed form, and these approximations cause systematic errors in the estimated orientation of the surface. We compare the systematic errors of the proposed method, linear moments method, and Buffon transform method using artificial data of orientation. As shown in Fig.6, the original data of orientation used in this experiment is made of 100 texture elements whose orientations are from a Gaussian distribution with a mean of 0 degrees and a standard deviation of 30 degrees. The proposed method requires two sets of data derived from the two different scales. In this experiment we randomly divided the original orientation data into two, and used them for the computation of the proposed method. First, we investigate the systematic error in slant angle changing the slant angle from 0 to 40 degrees with constant tilt angle of 45 degrees. Next, we investigate the systematic error in tilt angle changing the tilt angle from 0 to 90 degrees with a constant slant angle of 30 degrees.

Fig.7 (a) and (b) show the systematic error in the slant and tilt angles of the proposed method (solid lines), linear moments method (dashed lines) and Buffon transform method (dash-dot lines). The proposed method exhibits the best accuracy in slant angle and good accuracy in tilt angles, independent of the slant and tilt angles, although the accuracy of Buffon transform method degrades rapidly with slant and tilt angles.

4.2 Comparison of Noise Sensitivity

Next we compare the noise sensitivities of these three methods. Random Gaussian noise with a standard deviation of 1.0 degree was added to the orientation data of the texture elements used in the above experiments. The errors in slant and tilt angle caused by the random Gaussian noise are shown in Fig.8 (a) and (b).

Although all methods are sensitive to noise in the case of small slant, the slant estimated by the proposed method is less affected by noise than that of the other methods. As shown in Fig.8 (b), all methods have similar noise sensitivity with respect to the tilt angle.

Although the accuracy and noise sensitivity change in terms of the type of texture, the proposed method is more accurate and less sensitive to noise in most of the cases. Further more, it makes the advantage of the proposed method clear that the linear moments method suffers from an aliasing problem as explained before, and Buffon transform method cannot compute one of the four components of an affine transformation, the change in scale.

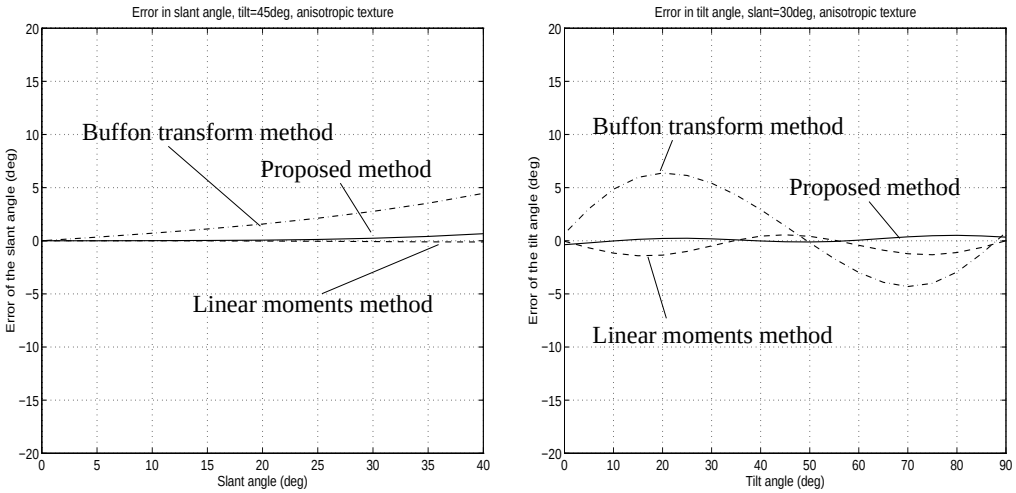

(a) (b)

Figure 7: Results of systematic error analysis. (a) and (b) show the errors in the estimation of the slant and tilt angles of the surface. The solid line, dashed line and dash-dot line show the error of the proposed method, linear moments method [30] and Buffon transform method [26] respectively. This systematic error arises from the small deformation approximation required to linearize the equation for a closed form solution.

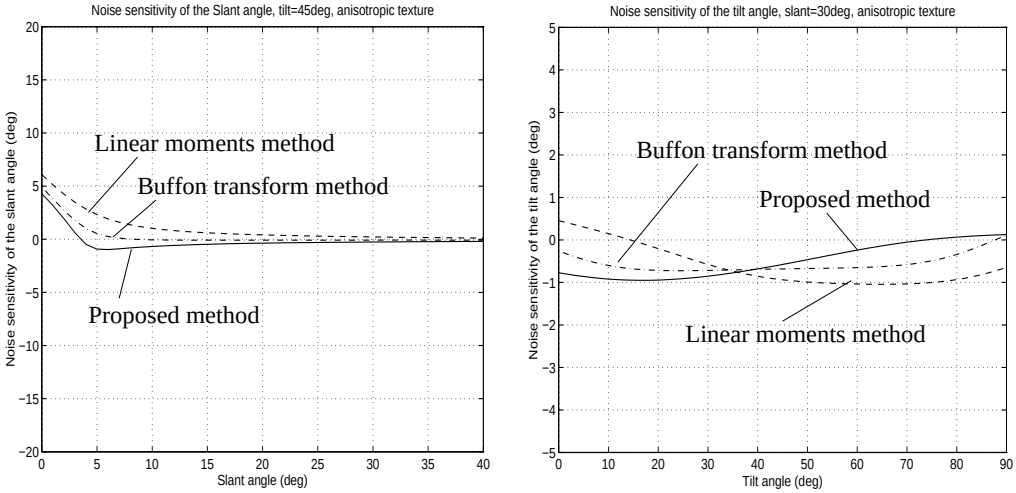

(a) (b)

Figure 8: Results of noise sensitivity analysis. (a) and (b) show errors in slant and tilt angle of the surface caused by additive Gaussian noise with standard deviation of 1.0 degree. The solid line, dashed line and dash-dot line show the noise sensitivity of the proposed method, linear moments method, and Buffon transform method respectively.

5 Experiments

In this section, we present results which show that this method does not need any assumptions like directional isotropy or spatial homogeneity to estimate the four components of the affine transformation. To demonstrate the accuracy of the extracted affine transform, we have chosen to assume that the original images are of textures on a fronto-parallel plane, and we use the affine transformation to estimate the motion of the plane, that is change in orientation and distance of the plane, assuming it is viewed under *weak* perspective. The relationship between the plane motion and the differential invariants of the image velocity field can be described as follows (see Appendix C for derivation):

$$\begin{aligned} r &= \frac{1}{1+s+\sqrt{d_1^2+d_2^2}} \\ \theta &= c \\ \tan 2\tau &= \frac{d_2}{d_1} \\ \cos\sigma &= 1-2\sqrt{d_1^2+d_2^2} \end{aligned}$$

In practice, we have used isotropic diffusion to derive multi-scale images. Although isotropic diffusion does not in general preserve an affine transformation and may cause systematic error in the orientation of the texture elements, we have found experimentally that the distortion of the texture elements caused by an isotropic diffusion is small and the systematic error in orientation is negligible (see Fig.9).

In the first experiment, the original image of artificial texture elements is deformed by an affine transformation which is equivalent to the three dimensional motion of a fronto-parallel surface with a slant angle of 30 degrees, a tilt angle of 60 degrees and a relative change in distance of 1.1. Two sets of original and deformed scale-space images shown in the top row of Fig.10 are made using isotropic diffusion with scales (variances) of $\sigma^2 = 0$ and $\sigma^2 = 30$ respectively. The four images in the second row of Fig.10 show edges obtained by the edge detector from the images in the top row. The moments of the original and deformed texture elements are computed from the orientation of the image feature at each edge point. The affine transformation is computed from the proposed method and used to compute the three dimensional motion of the textured surface. The center and right ellipses in Fig.10 show the calibrated and estimated orientation and the change in distance of the textured surface using distortion of the shape from the original circle shown in the left. Fig.11 shows the results from this method tested on a stained glass image, which is distorted by an affine transformation equivalent to a three dimensional rotation with slant and tilt angle of 30 and 120 degrees. Fig.12 shows the results from a Big Ben image, which is distorted by an affine transformation equivalent to a three dimensional rotation with slant and tilt angle of 30 and 45 degrees. The ellipses in Fig.10, Fig.11 and Fig.12 show that the estimated orientations and the change in distance are qualitatively good even with non-uniform and anisotropic textures.

Table1 compares the accuracy of this method quantitatively for each sample image with the known fiducial orientation. The errors seen in the case of the stained glass image and the Big Ben image are mainly caused by: (1) The difference of the sampling points between the original and deformed images, that is the sampling error and the difference of the area of interest between the two images. (2) In this experiment, we used isotropic diffusion for simplicity. Isotropic diffusion, however, does not always preserve an affine transformation and may cause systematic error in the orientation of the texture elements. This problem can be avoided by using an affine invariant scale-space which preserves an affine transformation [35, 36].

In this experiment, we chose the scales of multi-scale representation manually. In practice, however, selection of scales affects the accuracy of computation of an affine transformation. The sensitivities to selection of scales have to be analyzed in future work.

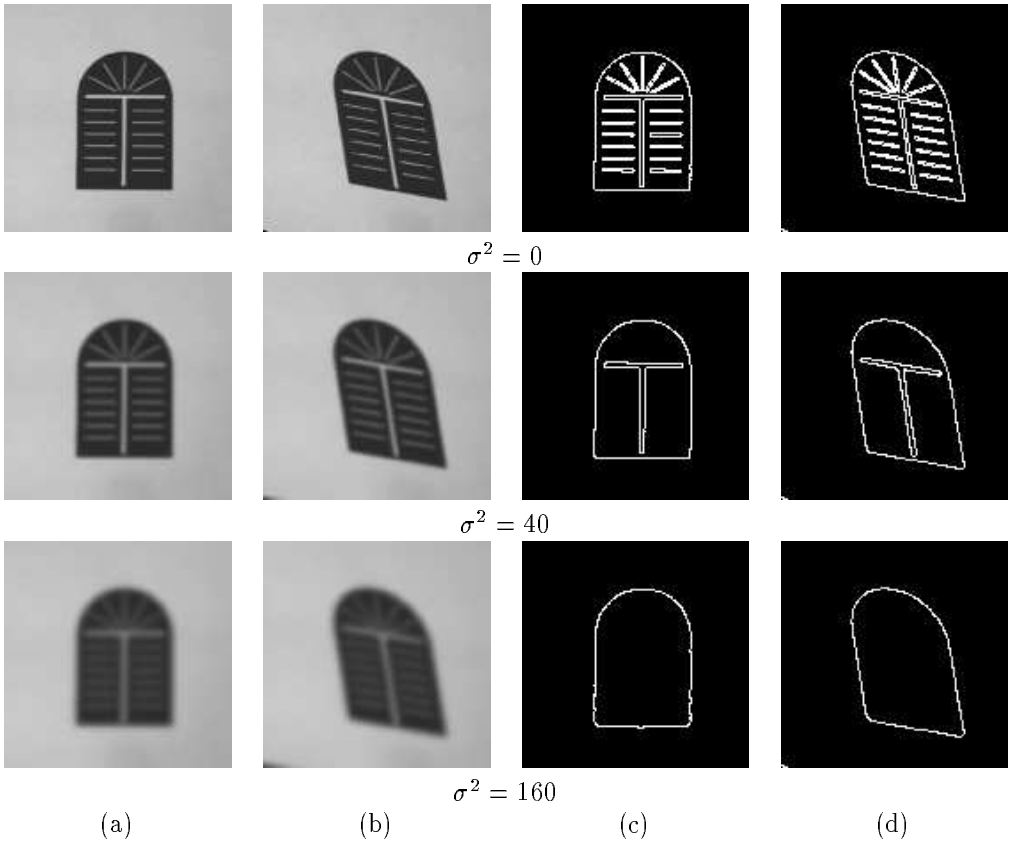

Figure 9: Original and distorted multi-scale images and their edges. The images in the second and third row of columns (a) and (b) are derived from the images in the top row by isotropic diffusion with scales (variances) of $\sigma^2 = 40$ and $\sigma^2 = 160$ respectively. The images in columns (c) and (d) show edges derived from the images in columns (a) and (b) respectively. Comparing with Fig.3, we find that the distortion of the texture elements caused by an isotropic diffusion is small and negligible.

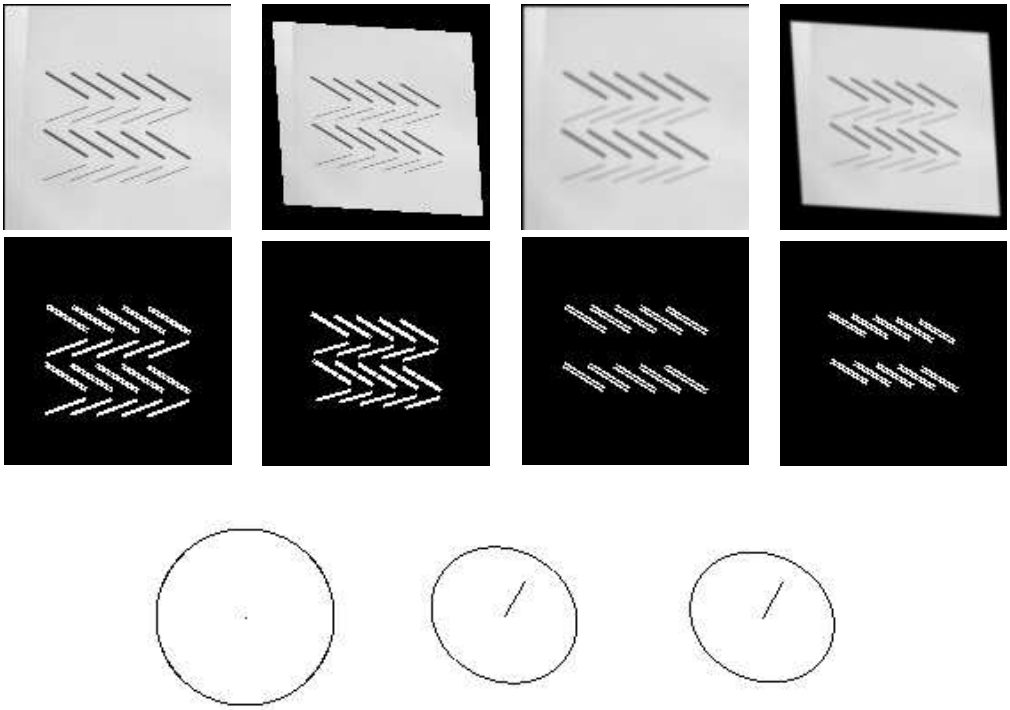

Figure 10: Results of preliminary experiments (artificial texture image). Examples of the images distorted by an affine transformation equivalent to a three dimensional motion with a slant angle of 30 degrees, a tilt angle of 60 degrees and a change in distance of 1.1, were processed by our affine transform from texture moments algorithm. Images in the top row are the original and distorted images of scale (variance) $\sigma^2 = 0$, and the original and distorted images of scale $\sigma^2 = 30$. Images in the second row show the edges detected from the images in the top row. These images show that different scale-space representations have different image structures. The center and right ellipses in the third row show the real and estimated orientation and the change in distance using normal vectors and oriented circles whose size and shape correspond to the scale change and distortion from the original fronto-parallel circle shown in the left.

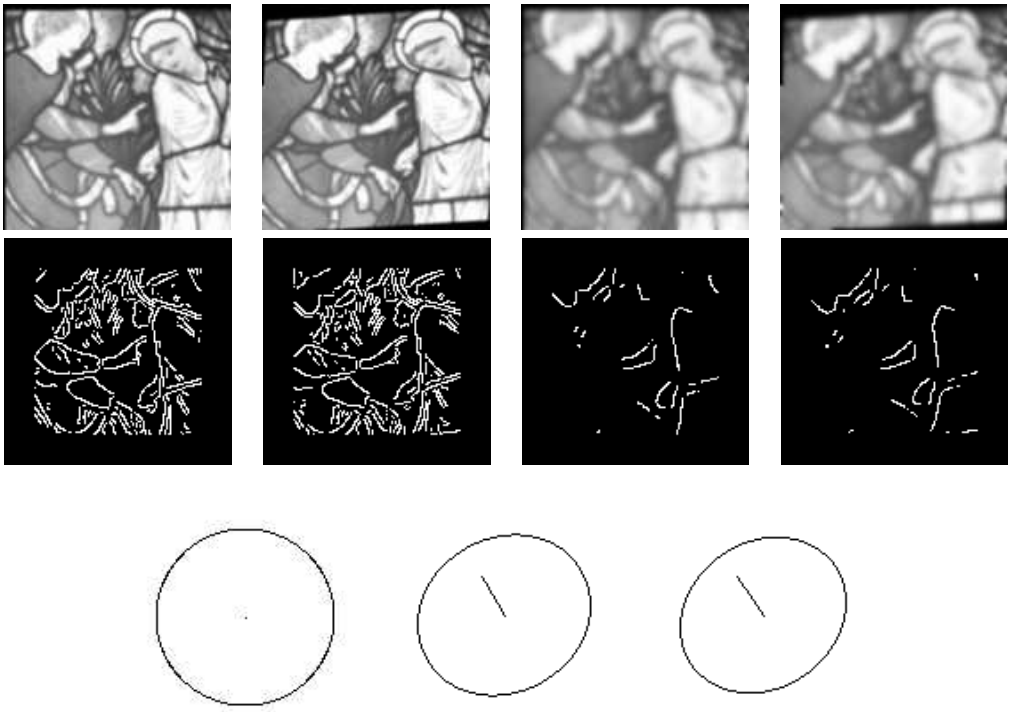

Figure 11: Results of preliminary experiments (stained glass image). Examples of the images distorted by an affine transformations equivalent to a three dimensional rotation with a slant angle of 30 degrees and a tilt angle of 120 degrees, were processed by our affine transform from texture moments algorithm. Images in the top row are the original and distorted images of scale (variance) $\sigma^2 = 30$, and the original and distorted images of scale $\sigma^2 = 200$. Images in the second row show the edges detected from the images in the top row. The center and right ellipses in the third row show the real and estimated orientation and the change in distance.

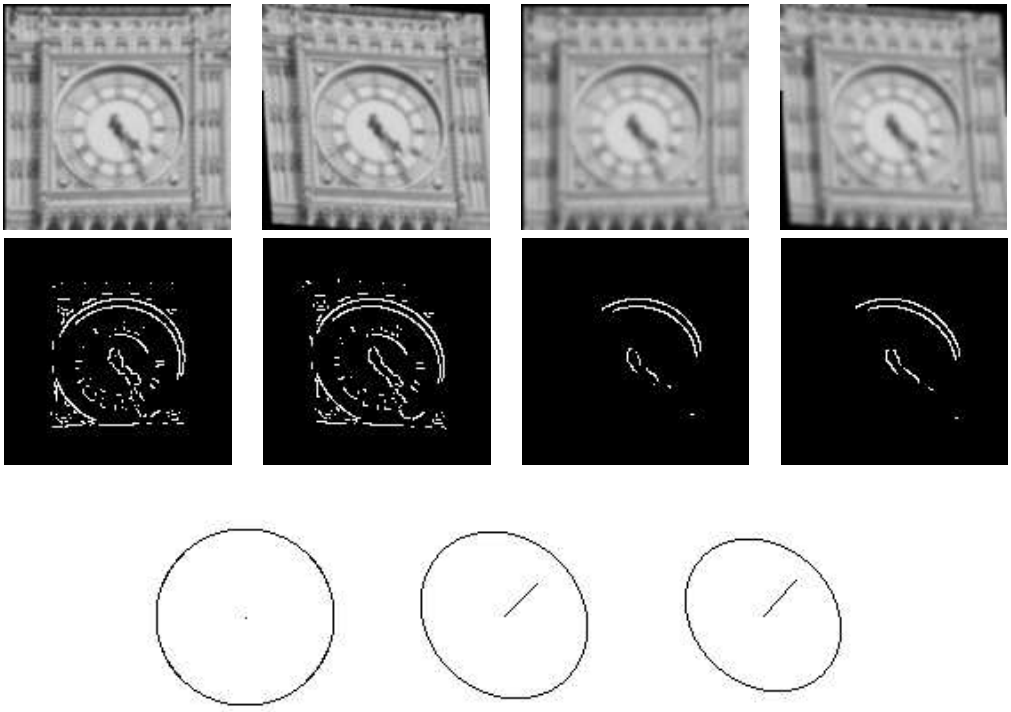

Figure 12: Results of preliminary experiments (Big Ben image). Examples of the images distorted by an affine transformations equivalent to a three dimensional rotation with a slant angle of 30 degrees and a tilt angle of 45 degrees, were processed by our affine transform from texture moments algorithm. Images in the top row are the original and distorted images of scale (variance) $\sigma^2 = 30$, and the original and distorted images of scale $\sigma^2 = 100$. Images in the second row show the edges detected from the images in the top row. The center and right ellipses in the third row show the real and estimated orientation and the change in scale.

Table 1: Accuracy of the estimated surface motion: changes in distance, r, rotation, θ, tilt, τ, and slant, σ which are computed from the differential invariants, s, c, d_1, d_2.

Images		r	$\theta(^\circ)$	$\tau(^\circ)$	$\sigma(^\circ)$
	True	1.10	0.0	60.0	30.0
(a) **artificial texture**	Estimated	1.12	0.3	61.1	31.9
	True	1.00	0.0	120.0	30.0
(b) **stained glass**	Estimated	0.97	0.6	123.5	32.4
	True	1.00	0.0	45.0	30.0
(c) **Big Ben**	Estimated	0.94	-0.2	48.4	33.4

6 Conclusion

In this paper we have proposed a novel method to compute the four components of an affine transformation from the changes in circular moments of edge orientation. A method to combine the moments of the texture image and the scale-space representation is described. This method does not require any point, edge or contour correspondences to be established, and is simple and efficient. The estimated affine transformation is accurate enough to be useful in shape from texture and visual navigation. We hope to exploit the information derived from the proposed method in computing surface orientation and time-to-contact for the visual navigation of a mobile robot [16]. The remaining problems are:

1. The proposed method relies on the comparison of statistics of the image patches. This will only be meaningful if the two patches are projections of "world" textures with similar properties. This therefore requires that corresponding areas of interest are identified.
2. Although we can choose any two different scales from the scale-space representation to compute an affine transformation in the proposed method, the selection of scale affects the accuracy of the estimated affine transformation. How to choose the best scales to raise the accuracy and robustness of the proposed method remains a problem.
3. In this paper we described a method which requires minimal information, that is two different scales. However, we can of course use more than two scales to raise the accuracy and robustness of the method.

Appendix A

From (3) the length $L'(\varphi)$ can be described by:

$$\begin{aligned} L'(\varphi)^2 &= ((1+s+d_1)\cos\varphi + (d_2-c)\sin\varphi)^2 + \\ &\quad ((d_2+c)\cos\varphi + (1+s-d_1)\sin\varphi)^2 \\ &= 2(d_1+d_1 s+d_2 c)\cos 2\varphi + 2(d_2+d_2 s-d_1 c)\sin 2\varphi + \\ &\quad 1+d_1^2+d_2^2+c^2+s^2+2s \end{aligned} \tag{20}$$

If the image distortion is small, the differential invariants, s, c, d_1, d_2 are small enough to neglect the second order products of these differential invariants. Then, (20) is approximated to first order by:

$$L'(\varphi)^2 \simeq 1+\lambda$$

where:

$$\lambda = 2d_1 \cos 2\varphi + 2d_2 \sin 2\varphi + 2s$$

Because $\lambda \ll 1$ under small image distortion, the length, $L'(\varphi)$, can be approximated by:

$$\begin{aligned} L'(\varphi) &\simeq 1 + \frac{1}{2}\lambda \\ &\simeq 1 + d_1 \cos 2\varphi + d_2 \sin 2\varphi + s \end{aligned}$$

Appendix B

From (11), odd order ((2k+1)-th) circular moments, $I_{\sin(2k+1)\varphi}$, are described as follows:

$$I_{\sin(2k+1)\varphi} = \int_0^{2\pi} \sin((2k+1)\varphi) f(\varphi) d\varphi$$

Dividing the interval into $(0, \pi)$ and $(\pi, 2\pi)$:

$$\begin{aligned} I_{\sin(2k+1)\varphi} &= \int_0^{\pi} \sin((2k+1)\varphi) f(\varphi) d\varphi + \int_{\pi}^{2\pi} \sin((2k+1)\varphi) f(\varphi) d\varphi \\ &= \int_0^{\pi} \sin((2k+1)\varphi) f(\varphi) d\varphi + \\ &\quad \int_0^{\pi} \sin((2k+1)(\varphi+\pi)) f(\varphi+\pi) d\varphi \end{aligned} \tag{21}$$

Because φ and $\varphi + \pi$ cannot be distinguished, $f(\varphi)$ and $f(\varphi + \pi)$ are exactly the same. Therefore, from (21):

$$\begin{aligned} I_{\sin(2k+1)\varphi} &= \int_0^{\pi} \sin((2k+1)\varphi) f(\varphi) d\varphi + \int_0^{\pi} \sin((2k+1)(\varphi+\pi)) f(\varphi) d\varphi \\ &= \int_0^{\pi} \sin((2k+1)\varphi) f(\varphi) d\varphi - \int_0^{\pi} \sin((2k+1)\varphi) f(\varphi) d\varphi \\ &= 0 \end{aligned}$$

Similarly, $I_{\cos(2k+1)\varphi}$ are also zero. On the other hand, even order (2k-th) circular moments, $I_{\sin 2k\varphi}$, can be described as follows:

$$\begin{aligned} I_{\sin 2k\varphi} &= \int_0^{2\pi} \sin(2k\varphi) f(\varphi) d\varphi \\ &= \int_0^{\pi} \sin(2k\varphi) f(\varphi) d\varphi + \int_{\pi}^{2\pi} \sin(2k\varphi) f(\varphi) d\varphi \\ &= \int_0^{\pi} \sin(2k\varphi) f(\varphi) d\varphi + \int_0^{\pi} \sin(2k(\varphi+\pi)) f(\varphi+\pi) d\varphi \\ &= \int_0^{\pi} \sin(2k\varphi) f(\varphi) d\varphi + \int_0^{\pi} \sin(2k\varphi) f(\varphi) d\varphi \\ &= 2\int_0^{\pi} \sin(2k\varphi) f(\varphi) d\varphi \end{aligned}$$

Similarly, $I_{\cos 2k\varphi}$ are:

$$I_{\cos 2k\varphi} = 2\int_0^{\pi} \cos(2k\varphi) f(\varphi) d\varphi$$

Appendix C

If the original images are of textures on a fronto-parallel plane under weak perspective, the affine transformation which describes the image distortion caused by the three dimensional motion of the plane can be decomposed into each component of the plane motion, that is the change in distance, S, rotation, R, with axis perpendicular to the image, and shear, D, caused by a rotation with axis parallel to the image [24]:

$$A = SRD$$

where, S is specified by a relative change in distance, r, R is specified by a rotation angle, θ, D is specified by a tilt angle, τ, and a slant angle, σ:

$$\begin{aligned} S(r) &= \begin{bmatrix} \frac{1}{r} & 0 \\ 0 & \frac{1}{r} \end{bmatrix} \\ R(\theta) &= \begin{bmatrix} \cos\theta & -\sin\theta \\ \sin\theta & \cos\theta \end{bmatrix} \\ D(\tau,\sigma) &= \begin{bmatrix} \cos\tau & -\sin\tau \\ \sin\tau & \cos\tau \end{bmatrix} \begin{bmatrix} \cos\sigma & 0 \\ 0 & 1 \end{bmatrix} \begin{bmatrix} \cos\tau & \sin\tau \\ -\sin\tau & \cos\tau \end{bmatrix} \end{aligned}$$

If the image distortion is small, the affine transformation, A, can be approximated to first order as follows:

$$\begin{aligned} A &= (I + \Delta S)((I + \Delta R)(I + \Delta D) \\ &\simeq I + \Delta S + \Delta R + \Delta D \end{aligned} \tag{22}$$

where:

$$\begin{aligned} \Delta S &= \begin{bmatrix} \frac{1}{r} - 1 & 0 \\ 0 & \frac{1}{r} - 1 \end{bmatrix} \\ \Delta R &= \begin{bmatrix} \cos\theta - 1 & -\sin\theta \\ \sin\theta & \cos\theta - 1 \end{bmatrix} \\ \Delta D &= \begin{bmatrix} \cos\tau & -\sin\tau \\ \sin\tau & \cos\tau \end{bmatrix} \begin{bmatrix} \cos\sigma - 1 & 0 \\ 0 & 0 \end{bmatrix} \begin{bmatrix} \cos\tau & \sin\tau \\ -\sin\tau & \cos\tau \end{bmatrix} \end{aligned}$$

Further more, if the rotation, θ, is small, ΔR is approximated to first order as follows:

$$\Delta R \simeq \begin{bmatrix} 0 & -\theta \\ \theta & 0 \end{bmatrix}$$

Comparing (22) with (1), we can derive the relationship between the first order deferential invariants and the plane motion parameters as follows:

$$\begin{aligned} r &= \frac{1}{1 + s + \sqrt{d_1^2 + d_2^2}} \\ \theta &= c \\ \tan 2\tau &= \frac{d_2}{d_1} \\ \cos\sigma &= 1 - 2\sqrt{d_1^2 + d_2^2} \end{aligned}$$

References

[1] J.J. Gibson. *The Perception of the Visual World.* Houghton Mifflin, 1950.

[2] J.J. Koenderink and A.J. van Doorn. Invariant properties of the motion parallax field due to the movement of rigid bodies relative to an observer. *Optica Acta*, 22(9):773–791, 1975.

[3] J.J. Koenderink. Optic flow. *Vision Research*, 26(1):161–180, 1986.

[4] T. Kanade and J.R. Kender. Mapping image properties into shape constraints: Skewed symmetry, affine-transformable patterns, and the shape-from-texture paradigm. In J.Beck et al, editor, *Human and Machine Vision*, pages 237–257. Academic Press, NY, 1983.

[5] J. Malik and R. Rosenholtz. A differential method for computing local shape-from-texture for planar and curved surfaces. In *Proc. Conference on Computer Vision and Pattern Recognition*, pages 267–273, New York, 1993.

[6] K. Kanatani. Structure and motion from optical flow under orthographic projection. *Computer Vision, Graphics and Image Processing*, 35:181–199, 1986.

[7] L. Dreschler and H.H. Nagel. Volumetric model and 3D trajectory of a moving car derived from monocular TV-frame sequence of a street scene. In *Proc. International Joint Conference on Artificial Intelligence*, pages 692–697, 1981.

[8] L. Kitchen and A. Rosenfeld. Grey-level corner detection. *Pattern Recognition Letters*, 1:95–102, 1982.

[9] H.H. Nagel. Principles of (low level) computer vision. In J.P. Haton, editor, *Fundamentals in computer understanding: speech and vision*, pages 113–139. Cambridge University Press, 1987.

[10] C. Harris. Geometry from visual motion. In A. Blake and A. Yuille, editors, *Active Vision*, pages 263–284. MIT Press, Cambridge, USA, 1992.

[11] M. Brady and H. Wang. Vision for mobile robots. *Philosophical Transactions of the Royal Society of London, Series B*, 337:341–350, 1992.

[12] I.D. Reid and D.W. Murray. Tracking foveated corner clusters using affine structure. In *Proc. 4th International Conference on Computer Vision*, pages 76–83, Berlin, 1993.

[13] J.F. Canny. A computational approach to edge detection. *IEEE Trans. Pattern Analysis and Machine Intelligence*, 8:679–698, 1986.

[14] D. Murray and B. Buxton. *Experiments in the machine interpretation of visual motion.* MIT Press, Cambridge, USA, 1990.

[15] H.S. Sawhney and A.R. Hanson. Identification and 3D description of 'shallow' environmental structure in a sequence of images. In *Proc. Conference on Computer Vision and Pattern Recognition*, pages 179–185, Lahaina, 1991.

[16] R. Cipolla and A. Blake. Surface orientation and time to contact from image divergence and deformation. In G. Sandini, editor, *Proc. 2nd European Conference on Computer Vision*, pages 187–202, Santa Margherita, Italy, 1992. Springer–Verlag.

[17] P. Anandan. A computational framework and an algorithm for the measurement of visual motion. *International Journal of Computer Vision*, 2(3):283–310, 1989.

[18] J.R. Bergen, P. Anandan, K.J. Hanna, and R. Hingorani. Hierarchical model-based motion estimation. In G. Sandini, editor, *Proc. 2nd European Conference on Computer Vision*, pages 237–252, Santa Margherita, Italy, 1992. Springer–Verlag.

[19] B.D. Lucas and T. Kanade. An iterative image registration technique with an application to stereo vision. In *Proc. International Joint Conference on Artificial Intelligence*, pages 674–679, 1981.

[20] D.G. Jones and J. Malik. Determining three-dimensional shape from orientation and spatial frequency disparities. In G. Sandini, editor, *Proc. 2nd European Conference on Computer Vision*, pages 661–669, Santa Margherita, Italy, 1992. Springer–Verlag.

[21] R. Bajcsy and L. Lieberman. Texture gradient as a depth cue. *Computer Graphics and Image Processing*, 5:52–67, 1976.

[22] B.J. Super and A.C. Bovik. Solution to shape-from-texture by wavelet-based measurement of local spectral moments. In *Proc. Conference on Computer Vision and Pattern Recognition*, 1992.

[23] A.P. Witkin. Recovering surface shape and orientation from texture. *Artificial Intelligence*, 17:17–45, 1981.

[24] A. Blake and C. Marinos. Shape from texture: estimation, isotropy and moments. *Artificial Intelligence*, 45:323–380, 1990.

[25] L.G. Brown and H. Shyvaster. Surface orientation from projective foreshortening of isotropic texture autocorrelation. *IEEE Trans. Pattern Analysis and Machine Intelligence*, 12(6):584–588, 1990.

[26] K. Kanatani. Detection of surface orientation and motion from texture by a stereological technique. *Artificial Intelligence*, 23:213–237, 1984.

[27] T. Lindeberg and J. Garding. Shape from texture from a multi-scale perspective. In *Proc. 4th International Conference on Computer Vision*, pages 683–691, Berlin, 1993.

[28] J. Garding and T. Lindeberg. Direct computation of shape cues by multi-scale retinotopic processing. *Technical Report, Royal Institute of Technology, TRITA-NA-P9304*, 1993.

[29] A.M. Waxman and K. Wohn. Contour evolution, neighbourhood deformation and global image flow: planar surfaces in motion. *International Journal of Robotics Research*, 4(3):95–108, 1985.

[30] J. Sato and R. Cipolla. Extracting the affine transformation from texture moments. In Jan-Olof Eklundh, editor, *Proc. 3rd European Conference on Computer Vision*, volume 2, pages 165–172, Stockholm, 1994. Springer–Verlag.

[31] J.J. Koenderink. The structure of images. *Biological Cybernetics*, 50:363–370, 1984.

[32] T. Lindeberg. Detecting salient blob-like image structures and their scales with a scale-space primal sketch: A method for focus-of-attention. *International Journal of Computer Vision*, 11(3):283–318, 1993.

[33] A.P. Witkin. Space-scale filtering. In *Proc. International Joint Conference on Artificial Intelligence*, pages 1019–1022, 1983.

[34] P. Perona and J. Malik. Scale-space and edge detection using anisotropic diffusion. *IEEE Trans. Pattern Analysis and Machine Intelligence*, 12(7):629–639, 1990.

[35] C. Lopez and J.M. Morel. Axiomatization of shape-analysis and application to texture hyperdiscrimination. In *Proc. Conference on Computer Vision and Pattern Recognition*, pages 646–647, New York, 1993.

[36] G. Sapiro and A. Tannenbaum. Affine invariant scale-space. *International Journal of Computer Vision*, 11(1):25–44, 1993.

[37] K.V. Mardia. *Statistics of directional data*. Academic Press, London, 1972.